

Heterogeneous Combustion of Benzene on Rh(111): Kinetics and Dynamics of CO and CO₂ Production

M. E. Viste, K. D. Gibson, and S. J. Sibener¹

The James Franck Institute and Department of Chemistry, The University of Chicago, 5640 South Ellis Avenue, Chicago, Illinois 60637

Received September 27, 1999; revised December 1, 1999; accepted December 13, 1999

The heterogeneous combustion of benzene on Rh(111) has been examined using molecular beams in an ultrahigh vacuum environment. For the reaction conditions studied, CO is the dominant carbon-containing product. CO₂ is a minor component, accounting for a maximum of 10% of the carbon species at 650 K and dropping to 2% when the temperature is raised to 1000 K. The relative yields of CO and CO₂, as well as the reaction rate for CO production, are strongly influenced by surface oxygen concentration, controlled through the relative ratio of oxygen and benzene fluxes, with the fastest rate of CO production and the greatest proportion of CO₂ occurring under the most oxidizing conditions. Because the catalytic decomposition of benzene is rapid on the rhodium surface, the kinetics of CO and CO₂ evolution are dominated by the reaction of atomic carbon and oxygen species on the surface. We calculate an activation energy for the reaction C(a) + O(a) → CO(a) of 130 kJ/mol. CO₂ is produced by the further reaction of CO with adsorbed O, with the extent of reaction being substantially influenced by reaction at defect sites. CO is evolved with a thermal kinetic energy distribution, while CO₂ desorbs hyperthermally.

© 2000 Academic Press

Key Words: rhodium; benzene; heterogeneous combustion; partial oxidation; surface reaction kinetics and dynamics; gas-surface reactive scattering; molecular beams.

INTRODUCTION

The combustion of aromatic hydrocarbons is of fundamental interest and practical importance in the production of useful synthetic products as well as in the disposal of undesirable fuel stream components by catalytic converters. Much work has been done to investigate the surface structure (1–6) and the oxidation and hydrogenation (7) of surface carbon from carbon monoxide (8–12) and methane (13–15), the components of syngas production, on a variety of metals including nickel, platinum, palladium, ruthenium, and rhodium. This research is relevant to the present investigation of benzene combustion on a rhodium surface because the decomposition of benzene on rhodium is quite

rapid; the kinetics of CO and CO₂ production are dominated by the reactions of surface carbon and oxygen. A key question in understanding the syngas reaction as well as benzene oxidation is the nature of the carbonaceous intermediate formed on the catalyst surface. On several metal surfaces, it is consistently found that carbonaceous compounds appear in carbide and graphitic forms. Carbide carbon is a monatomic surface species characterized by the similarity in Auger KVV line shape to that of transition metal carbides (15). Commonly formed at low coverages, carbide carbon is primarily bound to the metal surface, and it is the generally more reactive form. Graphitic carbon forms at high surface coverages and is characterized by strong carbon-carbon interactions that often render it nonreactive with surface hydrogen or oxygen. For this reason, the reaction is carried out under conditions of very low carbon coverage in the present study.

Koel and Somorjai have investigated the surface structures of benzene on Rh(111) (16). Using LEED and HREELS, they found that benzene adsorbs molecularly at 300 K. Temperature-programmed reaction studies find that it decomposes upon heating, with H₂ desorbing from the surface at 450 K and in a broader peak up to 680 K. They suggest that benzene decomposition on Rh(111) and on Ni (111), (110), (100) surfaces is initiated by carbon-carbon bond rupture to form the observed CH and C₂H species, in contrast to decomposition on Pd(111) and Pt(111) and (100) surfaces where carbon-hydrogen bonds are believed to break first. Above 500 K, at the near-monolayer coverages investigated, the carbon species on Rh(111) further dehydrogenate and polymerize to graphitic C_nH. Alstrup, investigating the interaction of hydrogen with carbide carbon on Ni(100), suggested that the transient formation of CH species facilitates carbon mobility (17).

Surface carbon reactivity is known to be influenced by carbon concentration on the surface and in the near-surface selvedge region of the catalyst. At the most basic level, high carbon concentration is associated with the formation of graphitic carbon which is unreactive because of the strong attraction between carbon atoms. On this basis, one might expect increasing carbon coverage to decrease reactivity.

¹ To whom correspondence should be addressed. Fax: (773) 702-5863.
E-mail: s-sibener@uchicago.edu.



Mikhailov (18) demonstrates a mild trend of this sort in an investigation of oxidation of carbon on a polycrystalline rhodium ribbon. The observed activation energy varied from 168 kJ/mol at $\Theta_C = 0.1$ ML to 185 kJ/mol at $\Theta_C = 0.5$ ML. In contrast, Alstrup's study (17) of the interaction of hydrogen with carbidic carbon on Ni(100) suggests that carbon sites are more reactive when the local carbon concentration is highest. He attributes this to local nickel surface reconstruction induced by the carbon adatoms. On palladium crystallite catalysts smaller than 25 nm, Borodzinski observes a positive correlation between the rate of acetylene hydrogenation catalysts and the bulk concentration of carbon (19), suggesting that even near-surface carbon concentrations can influence carbon reactivity.

The current study was conducted on a well-characterized Rh(111) surface in an ultrahigh vacuum environment. Multiple molecular beams (20, 21) were used to enable a detailed mechanistic study of hydrocarbon combustion kinetics and reaction dynamics. Previous related scattering experiments have been done by our group on the oxidation of carbon monoxide (22) and of hydrogen (23, 24), separate components of hydrocarbon oxidation. Carbon monoxide oxidation on Rh(111) depends on the surface concentration of oxygen and produces a bimodal kinetic energy distribution of carbon dioxide (22). This has been interpreted as involving both a thermal component and a second activated component, sharply peaked toward the surface normal with substantial energy release in the gaseous products. The oxidation of hydrogen by oxygen on Rh(111) was found to produce water which desorbed thermally with highly nonlinear kinetics (23). In studying benzene oxidation, we have extended the oxidation system to involve both the simultaneous formation of carbon dioxide and water and the oxidation of benzene to form carbon monoxide; we find that the hyperthermal character of the CO₂ is retained in the present system.

METHODS

As the apparatus has been described in detail elsewhere (25, 26), only the main features will be reviewed. Three separate molecular beams converge on a rhodium crystal in a UHV scattering chamber. Detection is via a differentially pumped quadrupole mass spectrometer collimated to have 1° angular resolution. The angle at which the incident beam strikes the surface and the final angle for product detection are independently adjustable. Chopper wheels are mounted both before and after the crystal to allow for waveform detection and velocity distribution measurement.

Three types of measurements were performed. First, using the postcrystal chopper, time-of-flight data were collected to determine product kinetic energies as a function of surface temperature. Then, by chopping the benzene beam before the crystal, reaction product waveforms were mea-

sured to investigate on-surface reaction kinetics. Finally, by slowing the prechopper so that background could be subtracted from the steady-state product signal, variations in product intensities and product ratios were measured as a function of surface temperature and reactant flux.

Dosing was done with two separate molecular beams, consisting of benzene and oxygen. The oxygen flux could be varied between 0.03 and 0.32 ML/s. (1 ML = 1.6×10^{15} molecules/cm².) Benzene was delivered to the molecular beam by bubbling argon through liquid benzene so that the total pressure was 4 psig. The benzene was typically cooled to 278 K to prevent condensation in the room temperature lines. The resulting benzene flux was estimated to be 0.01 to 0.02 ML/s.

Under these dosing conditions, the surface concentrations could be kept to a few percentage of saturation coverage. Most waveforms were taken twice so that early and late data could be compared: no temporal change in the waveforms was observed. From this waveform stability, and from the absence of oxygen in postreaction TPDs, we conclude that there is no buildup of surface or near-surface carbon or oxygen during the experiment.

RESULTS AND DISCUSSION

Reaction Products

The products CO, CO₂, and H₂O were observed, with CO strongly predominating over CO₂. While H₂ forms as well, the large mass 2 background in our detector precluded detailed study of this channel. Product intensities were measured for CO and CO₂. These were then adjusted to compensate for differences in ionizer sensitivity and product angular distributions so that product intensities could be meaningfully compared. Figure 1 displays relative intensities of CO to CO₂ as a function of oxygen/benzene flux ratio at 650 K (Fig. 1a) and as a function of temperature for a flux ratio of 14:1 (Fig. 1b). Figure 2 displays the reduced data as CO/CO₂ product ratios. The relative yield of CO/CO₂ decreases slightly with increasing O₂/benzene flux ratio (Fig. 2a) and increases linearly with temperature at constant flux ratio (Fig. 2b). This is consistent with a model in which CO is first formed on the surface and then either desorbs or reacts further with adsorbed oxygen. The reaction to form CO₂ therefore is favored by higher surface concentrations of oxygen present under higher oxygen flux ratios and is inhibited by lower surface residence times at higher temperatures.

Surface oxygen concentration influenced not only the CO/CO₂ product ratio, but also the kinetics for CO formation, which were investigated by observing time evolution waveforms for the CO product with three different reactant flux ratios. The use of modulated beam waveforms to investigate reaction kinetics has been described previously

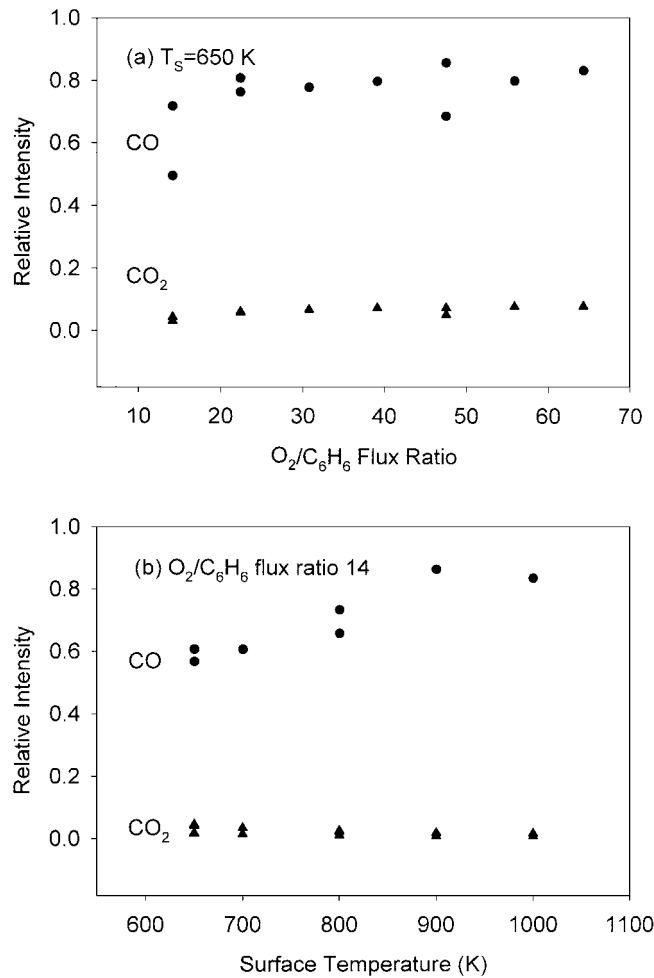


FIG. 1. CO and CO₂ product intensities. (a) Intensities as a function of incident oxygen/benzene flux ratios at $T_S = 650$ K. (b) Intensities as a function of surface temperature for a constant flux ratio of 14.

(20, 21, 27–29). Waveforms were strongly affected by different oxygen/benzene flux ratios, with the reaction becoming more rapid with higher oxygen flux, and hence with higher surface oxygen concentration. Changes in total flux at the same ratio had no strong effect on CO waveforms. Figure 3 shows four representative waveforms with three different flux ratios. Figure 3a compares waveforms with different oxygen/benzene flux ratio; these waveforms are distinctly different. Figure 3b compares waveforms of the same oxygen/benzene ratios, but different intensities. These waveforms exhibit very similar reaction rates.

CO Reaction Kinetics

To investigate the kinetics of carbon monoxide formation, CO waveforms were measured over a temperature range of 600 to 1100 K with three different oxygen/benzene flux ratios. Below 600 K, no continuous reaction was observed as unreactive carbon rapidly poisoned the surface.

Above 1100 K, the reaction kinetics were too fast to follow with the available chopper frequencies. Waveforms changed only slightly for CO upon changing chopping frequency; i.e., the kinetics involved were essentially linear.

We believe the kinetics of CO production are governed by the reaction of C and O on the rhodium surface. Previous work (16) has shown that benzene decomposes on Rh(111) at temperatures as low as 400 K to form CH and C₂H. Since the current study is undertaken at temperatures of 600 K and above, we expect this decomposition process to be rapid. In addition, temperature-programmed desorption studies (16) find that hydrogen continuously desorbs between 500 and 700 K, making it likely that the carbon is dehydrogenated in the temperature range of the current study. The overall reaction mechanism therefore involves a rapid series of reaction steps which break down the benzene reagent to carbidic carbon. C, H, and O are the primary expected surface adsorbates formed by reagent decomposition. These intermediates go on to produce OH,

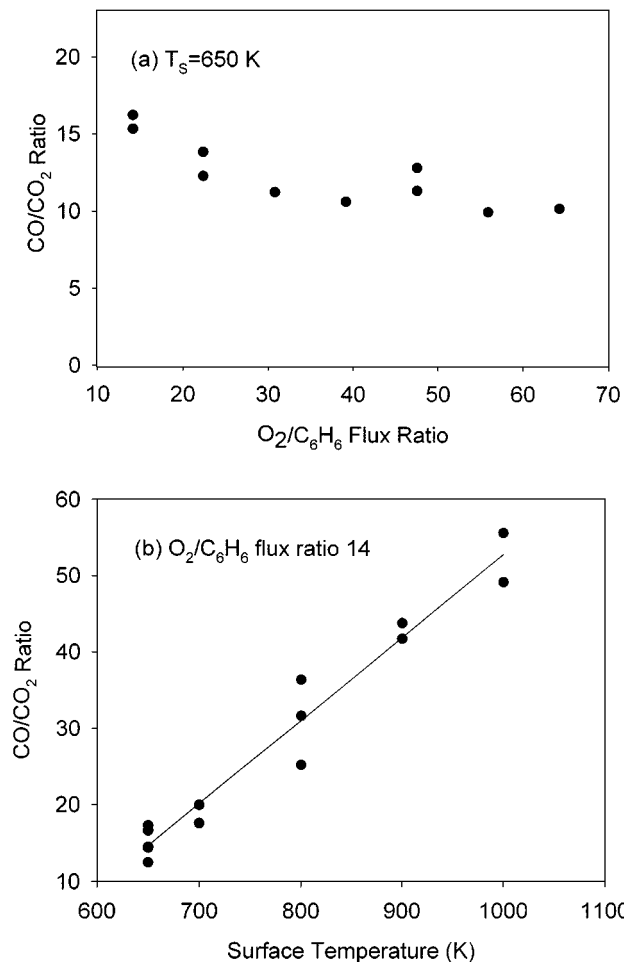


FIG. 2. CO/CO₂ product ratios. (a) Ratios as a function of incident beam flux ratios at $T_S = 650$ K. (b) Ratios as a function of temperature for an incident flux ratio of 14. The line is a guide to the eye.

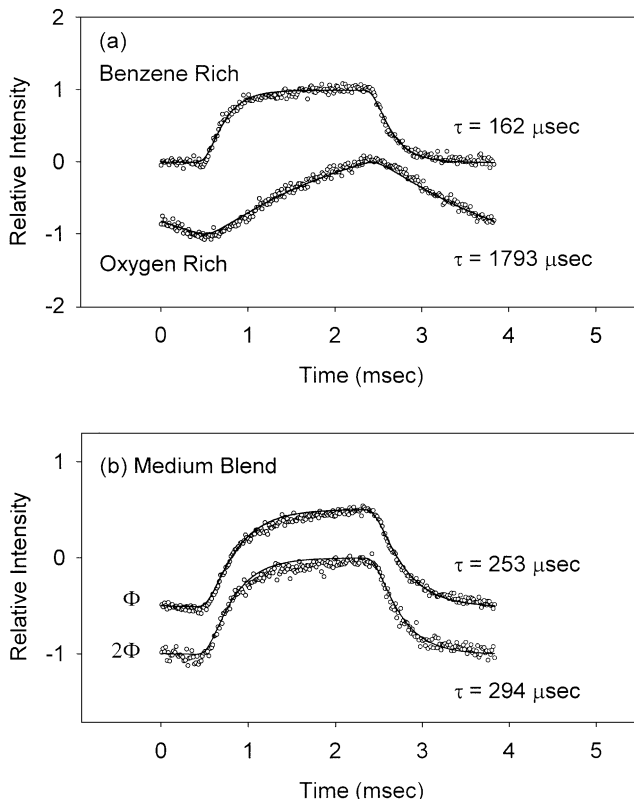


FIG. 3. CO waveforms for three different reactant flux ratios. (a) Waveforms are compared for conditions relatively rich in benzene (0.02 ML/s benzene and 0.16 ML/s oxygen fluxes) to conditions relatively rich in oxygen (0.01 ML/s benzene and 0.32 ML/s oxygen). The two waveforms exhibit substantially different rates, with characteristic rates of $\tau = 162$ and $\tau = 1793 \mu\text{sec}$ for benzene- and oxygen-rich conditions, respectively. (b) Waveforms are compared for the same oxygen/benzene flux ratio at two different total beam fluxes: Φ , 0.01 ML/s benzene and 0.16 ML/s oxygen, and 2Φ , 0.02 ML/s benzene and 0.32 ML/s oxygen. These waveforms are very similar with characteristic rates of $\tau = 253$ and $\tau = 294 \mu\text{sec}$.

H_2 , H_2O , CO, and CO_2 . Any of the carbonaceous species formed during decomposition might be expected to react with adsorbed oxygen. However, since the decomposition is rapid at elevated temperatures, and since surface concentrations are quite low, the dominant species is most likely adsorbed C.

CO waveforms were taken for toluene oxidation for comparison to those obtained for benzene oxidation. Temperature-programmed desorption of toluene oxidation has been shown to differ from that of benzene oxidation on palladium (30), yet the waveforms are sufficiently similar to suggest that the breakdown of toluene or benzene to carbon and hydrogen on the rhodium surface is fast compared to the oxidation of carbon. Thus, rapid benzene decomposition is followed by the reaction of adsorbed C and O to form CO. This latter step has the slowest rate and dominates the observed kinetics. Finally, surface carbon monoxide is desorbed or becomes further oxidized.

Mechanistic Studies Using Numerical Simulations

Since the signal is relatively weak and there is a high mass 28 background, the data are somewhat noisy. This makes Fourier analysis difficult. Another means of analysis is to propose a simplified mechanistic model for the surface reaction, and to do a forward convolution to fit the data.

The first thing to stress is that we are always working at low coverages. The chopper ran at modulation frequencies of 5–400 Hz, which only allowed exposure of the surface to the benzene beam for a fraction of a second. Results discussed here are only for cases where the CO signal has returned to baseline between successive openings of the chopper. This means that the baseline coverage of carbon on the surface is nil. The O_2 beam was continuous, but when we ran postreaction oxygen TPDs, we did not observe any measurable residual oxygen on the surface; $\Theta_{\text{O}} \leq 0.05 \text{ ML}$. We also took many spectra twice in succession without cleaning the surface between runs, and the spectra were identical. The model we propose predicts a substantial increase in the reaction rate as the oxygen coverage increases, supporting our conclusion that there is not much oxygen buildup.

The proposed reaction mechanism is summarized by the following differential equations,

$$\begin{aligned} \frac{d\Theta_{\text{O}}}{dt} &= S_{\text{O}} I_{\text{O}} (1 - 2\Theta_{\text{O}})^2 - k_1 \Theta_{\text{O}} \Theta_{\text{C}} \\ \frac{d\Theta_{\text{CO}}}{dt} &= k_1 \Theta_{\text{O}} \Theta_{\text{C}} - k_2 \Theta_{\text{CO}} \\ \frac{d\Theta_{\text{C}}}{dt} &= S_{\text{C}} I_{\text{C}} (1 - \Theta_{\text{C}}) - k_1 \Theta_{\text{O}} \Theta_{\text{C}}. \end{aligned}$$

Θ_{O} , Θ_{CO} , Θ_{C} are the surface concentrations of oxygen, carbon monoxide, and carbon, respectively. S_{O} and S_{C} are the sticking coefficients for oxygen and benzene. I_{O} and I_{C} are the incident intensities of oxygen and benzene. The rate constant k_1 represents the surface reaction of C and O to form CO, while k_2 is the rate constant for the desorption of CO from the surface. We estimated $S_{\text{O}} I_{\text{O}}$, the sticking coefficient times the flux for oxygen adsorption, from oxygen TPD spectra after short exposures of the clean Rh(111) to the O_2 beam. For the experiments reported here, this was between 0.021 and 0.045 ML/s. We also know that on clean Rh(111) the dissociative adsorption of O_2 follows a second order Langmuir isotherm (31). (Since the coverages of the reactants are always small, the exact form of the adsorption isotherm is unimportant.) From the work of Koel *et al.* (16), we know that benzene readily decomposes on Rh(111) at surface temperatures much lower than those used in these experiments, and we have treated the benzene beam as being a C source; the decomposition of benzene is instantaneous on the time scale of our measurements. $S_{\text{C}} I_{\text{C}}$, the sticking coefficient times the flux of carbon, can be estimated from a measurement of the total flux of the Ar/benzene beam and the vapor pressure of the benzene. It

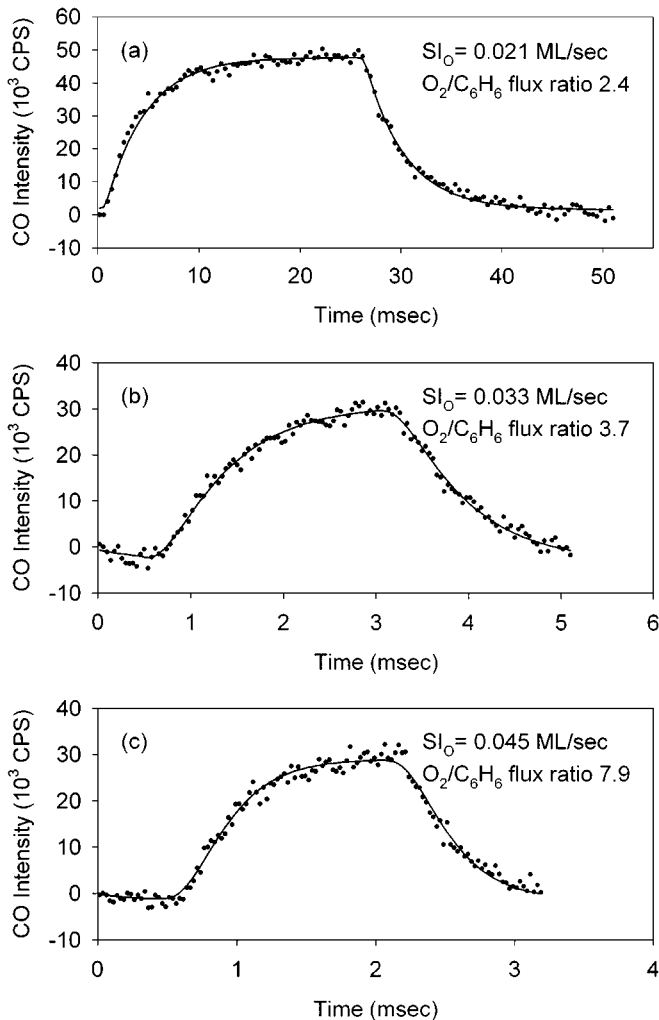


FIG. 4. Examples of data (circles) and fits (solid lines) for the three different oxygen fluxes, $T_S = 675\text{K}$.

can also be adjusted to prevent buildup of oxygen in the simulation. Either way, there is only a minor effect on the total reaction rate. Finally, we know the rate constant k_2 for the desorption of CO from the work of Peterlinz *et al.* (31, 32),

$$k_2 = v \cdot \exp\left(\frac{E_A}{RT_S}\right); \quad v = 2.54 \text{ s}^{-1}, E_A = 137.3 \text{ kJ/mol.}$$

This desorbing CO is what we detect.

The most critical input is the initial coverage of the reactants. As already noted, the initial coverage of carbon is $\Theta_C = 0 \text{ ML}$. Since the benzene beam is nearly constant, it would be reasonable that the oxygen coverage cannot be precisely 0 for the three fluxes used. So, for each flux, we allowed for a small quantity of adsorbed oxygen, increasing linearly with flux. The one variable that is then derived from fitting the numerical simulation to the data is k_1 , the rate of formation of adsorbed CO from adsorbed C and O.

We neglected the production of CO_2 because it is a minor product. The production of H_2O is another side reaction, but we do not feel that we know the kinetic parameters well enough to effectively include it in our modeling. The hydrogen is responsible for removing oxygen in excess of that needed to remove the carbon, thus preventing oxygen buildup on the surface.

The fitting procedure was to solve the above differential equations using a fourth-order Runge-Kutta integrator. The model synthetic waveforms so derived were convoluted with the appropriate velocity distributions and instrument functions to produce calculated waveforms which were then fit to the experimental data using a nonlinear least-squares fitting algorithm. Results for three different oxygen fluxes are shown in Fig. 4. Figure 5 shows Arrhenius plots for these results. The rate is strongly dependent on the initial value of Θ_O used, but the slopes are independent of this parameter.

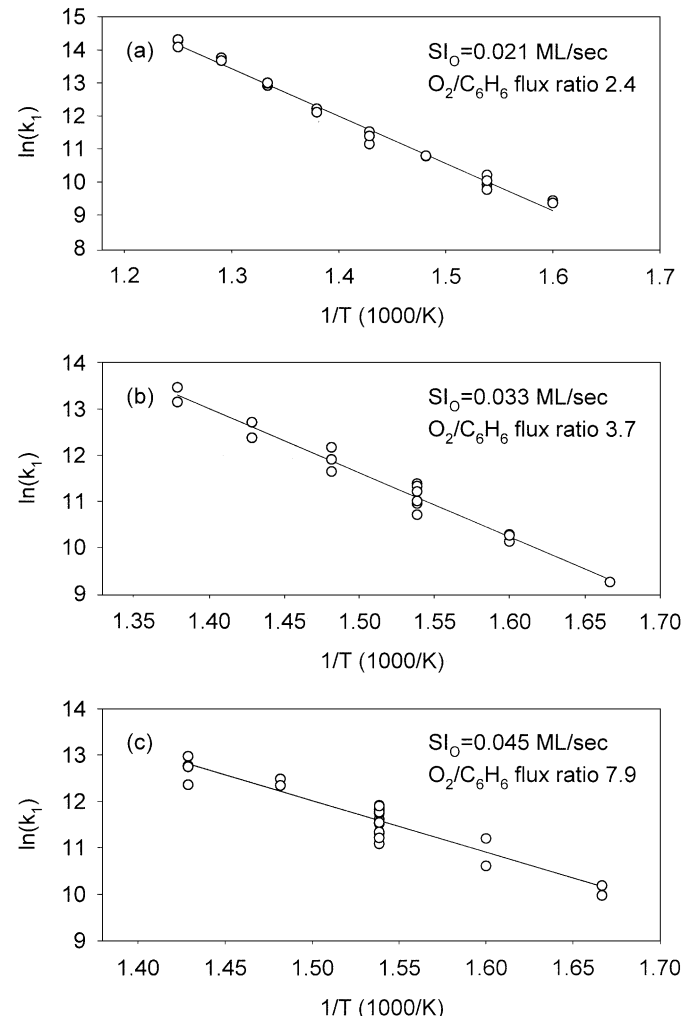


FIG. 5. Arrhenius plots for the reaction of adsorbed C plus O to form CO at the three different oxygen fluxes. The values of E_a , determined from the slopes, are (in kJ/mol) 133 ± 4.1 at $S_O I_O = 0.021 \text{ ML/s}$, 135.9 ± 8.0 at $S_O I_O = 0.033 \text{ ML/s}$, and 120 ± 11 at $S_O I_O = 0.045 \text{ ML/s}$.

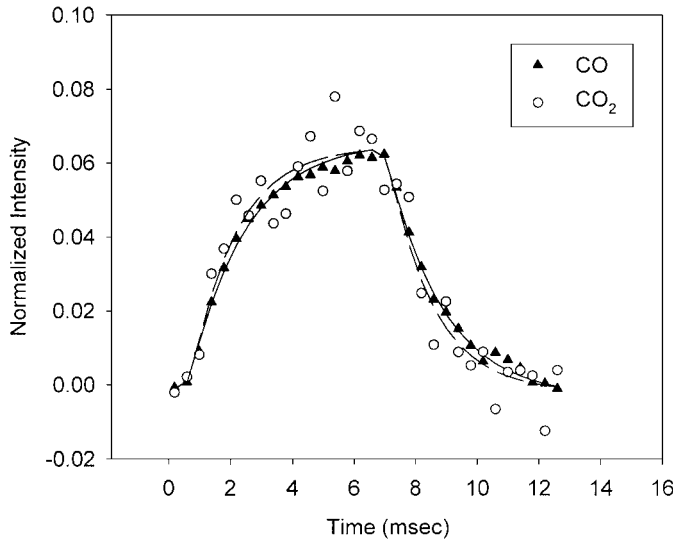


FIG. 6. CO and CO₂ waveform comparison: representative waveforms at $T_S = 650$ K and incident fluxes of 0.16 ML/s O₂ and 0.01 ML/s benzene for CO and CO₂, where the waveforms are normalized. The common shape of these waveforms supports a shared rate-limiting step for CO and CO₂ formation.

(Doubling Θ_O doubles the reaction rate.) We can therefore extract a value of the activation energy for the reaction of adsorbed C and O independent of assumptions about Θ_O , while quantifying the value of the preexponential factor is beyond the scope of our numerical analysis. The average value for the three reaction conditions used is ~ 130 kJ/mol, which is smaller than that previously reported for polycrystalline Rh(170 kJ/mol) (18) and Ni(100) (179 kJ/mol) (33); both of these studies were done at higher carbon coverages. Furthermore, carbon on rougher facets of the polycrystalline surface may be more highly coordinated to the rhodium surface and hence more tightly bound compared to carbon on the Rh(111) surface currently under investigation. Also, increases in carbon coverage would be expected to increase the activation energy due to surface carbon bonding changes associated with greater C-C interactions.

CO₂ Reaction Kinetics

Representative waveforms were obtained which were very similar to the CO waveforms, indicating that the same kinetically limiting step dominates both CO and CO₂ production. Figure 6 displays a normalized comparison of CO and CO₂ waveforms taken at $T_S = 650$ K. The production of CO₂ must therefore rely on a small fraction of the CO produced reacting with adsorbed oxygen prior to desorption. Since the CO oxidation is not influencing the kinetics, it must be rapid. Indeed, the activation energy of the CO(a) + O(a) \rightarrow CO₂(a) reaction on rhodium has been reported to be 103 kJ/mol (34), much less than we have calculated for carbon oxidation; this step is not rate limiting in the current study of benzene oxidation.

Thus, the simplest picture of the reaction of CO is that after being formed on the surface, it has a brief residence time during which the CO is thermalized and some fraction of it encounters oxygen with which it reacts to form CO₂. The observed CO/CO₂ ratio is never smaller than 10 and increases to about 50 at 1000 K. According to this model for CO₂ production, the ratio of CO/CO₂ should increase with increasing temperature as the CO residence time decreases, while it should decrease with increasing oxygen/benzene ratio at constant temperature as the relative surface concentration of reactive O increases. These trends are seen in Fig. 2. The relatively weak trend in relation to the oxygen/benzene ratio suggests that CO₂ is formed not only by reaction with oxygen atoms distributed randomly about the surface, where their concentration varies with incident oxygen flux, but that reaction at defect sites is responsible for a significant portion of the produced CO₂. Reaction of CO at the defect sites would not be limited by the diffusion of oxygen as the continuous flux of oxygen would tend to keep these sites saturated with trapped oxygen atoms.

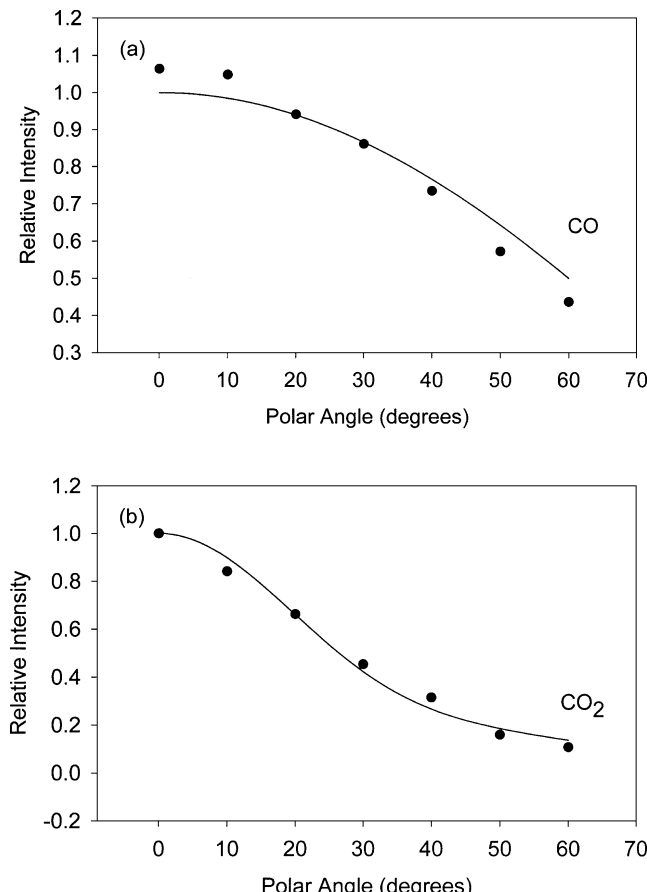


FIG. 7. CO and CO₂ angular distributions. (a) CO: The solid line is that for a thermal, i.e., cosine θ distribution. A least-squares fitting routine was used to scale the experimental data to the thermal distribution. (b) CO₂: The solid line is a fit to the angular distribution of Ref. (22) for the reaction of CO and O at $\Theta_O = 0.1$ ML, $0.27 \cos^{9.4}\theta + 0.73 \cos\theta$.

Product Angular and Energy Distributions

Figure 7 reports angular data from the CO and CO_2 desorption. The CO product distribution (Fig. 7a) is slightly peaked toward normal, $\sim \cos^{1.4} \theta$. The CO_2 distribution (Fig. 7b) is more sharply peaked. The solid line represents the fit to Colonell *et al.*'s CO_2 angular distribution (22), again at $\Theta_O = 0.1$ ML. This characterized the data well, further corroborating the model of surface reaction of CO and O to form CO_2 . Small deviations of the data from Colonell's fit might be expected from differences in surface oxygen concentration.

Figure 8 displays the translational energy derived from time-of-flight data for CO and CO_2 desorbing from the surface resulting from the benzene reaction. The solid line

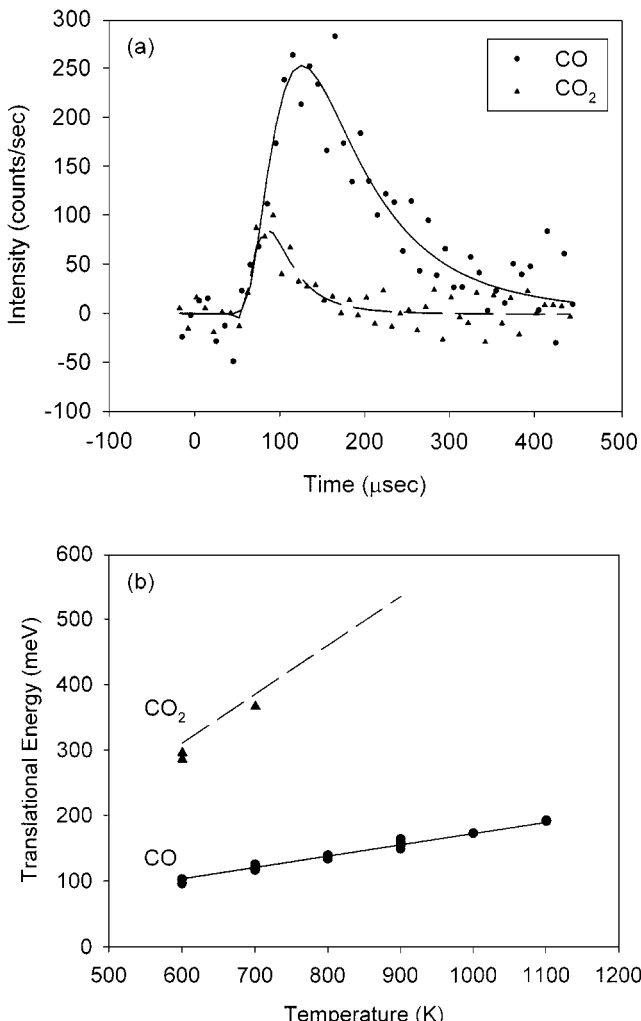


FIG. 8. (a) Time-of-flight distributions for CO and CO_2 desorbing from Rh(111) at $T_S = 600$ K. The fits shown are shifted Maxwell-Boltzmann distributions. The CO data were taken for 50 min, while the CO_2 data were collected for 65 min. (b) CO and CO_2 average translational desorption energies as a function of surface temperature. The solid line is the expected energy for thermal desorption. The dashed line represents the expected energy from the reaction of CO and O on Rh(111) at $\Theta_O = 0.1$ ML from Ref. (22).

represents an energy of $2kT$ characteristic of thermal desorption. The dashed line is $8.7kT - 139$ meV, taken from Colonell *et al.*'s earlier fit (22) for translational energy produced by CO oxidation to CO_2 at $\Theta_O = 0.1$ ML. The CO energy follows the thermal line very closely while the CO_2 energy follows the expected hyperthermal trend.

The potential energy surface for the CO reaction at defect sites is likely to be different from that involved in the reaction of CO observed by Colonell (22) for surface CO concentrations of 0.1 ML where the coverage was sufficiently high that the reaction was not dominated by defects. The binding energies of both CO and O are likely to be perturbed. Nevertheless, this need not interfere with the observed product translational energy. The high translational energy is associated with a late activation barrier, relatively far from the metal surface. Given this arrangement, the repulsive force felt by the products that sends them out sharply peaked at normal may not feel the irregularity of the defect. Alternatively, the defect sites might trap oxygen, perhaps nucleating a small, local oxygen island. In this case, the more concentrated oxygen region would be available at the defect sites while the actual oxidation would still occur on the bare rhodium surface.

CONCLUSIONS

The heterogeneous combustion of benzene on Rh(111) has been investigated under UHV conditions. The observed reaction rates are dominated by the oxidation of the adsorbed carbon deposited by the rapid decomposition of benzene to carbon and hydrogen. The CO product predominates over CO_2 by a factor of 15–50 over the range of temperatures we observed, becoming more dominant at higher temperatures. The CO/ CO_2 product ratio and the CO reaction kinetics are also both strongly influenced by the oxygen/benzene flux ratio. Higher oxygen ratios provide larger surface oxygen concentrations, which speed the reaction of CO and increase the relative yield of CO_2 . The reaction mechanism begins with the rapid decomposition of benzene on the rhodium surface to produce surface hydrogen, carbon and oxygen. The reaction of surface carbon and oxygen is found to be rate limiting for the production of both CO and CO_2 . CO_2 is formed by the further oxidation of a portion of the CO on the surface before it can desorb.

The kinetics of CO production have been analyzed by numerical integration of the relevant reaction steps. We assign an activation energy of $E_a = 130$ kJ/mol to the surface reaction of carbon and oxygen. This value is somewhat lower than the higher coverage ($\Theta_C = 0.2$ ML) value on polycrystalline rhodium of 170 ± 20 kJ/mol (18). This variation may result from attractive interactions between carbon atoms at higher coverage which hinder reaction. Additional attractive forces may also arise on the polycrystalline rhodium where exposed faces are more coordinating than

the very flat Rh(111), further contributing to a larger activation energy on the polycrystalline surface.

Angular distributions and velocity measurements reveal that CO desorbs thermally while CO₂ desorbs hyperthermally. The measured translational energies of the product CO₂ molecules arising from the benzene reaction agree well with those found in our earlier work for the oxidation of CO on Rh(111). The small amount of generated CO₂ depends only weakly on oxidizing conditions, suggesting that defect sites may play a substantial role in its production.

The heterogeneous combustion of benzene has been examined on Rh(111) using multiple molecular beams in an ultrahigh vacuum environment. These studies have revealed important aspects of the kinetics and dynamics for this prototypical aromatic reaction. The data thus generated join our prior studies of carbon monoxide and hydrogen oxidation on Rh(111), continuing to build a more comprehensive understanding of combustion-related chemistry on this technologically relevant catalytic surface.

ACKNOWLEDGMENTS

This work was supported by the AFOSR. M. E. Viste gratefully acknowledges a National Science Foundation Fellowship.

REFERENCES

- Yates, J. T., Williams, E. D., and Weinberg, W. H., *Surf. Sci.* **91**, 562 (1980).
- Rebholz, M., Prins, R., and Kruse, N., *Surf. Sci. Lett.* **259**, L797 (1991).
- de Koster, A., and van Santen, R. A., *Surf. Sci.* **233**, 366 (1990).
- Paul, J. F., and Sautet, P., *J. Phys. Chem B* **102**, 1578 (1998).
- Smirnov, M. Yu., and Zemlyanov, D. Yu., *Catal. Lett.* **8**, 101 (1991).
- Tian, Z., Dewaele, O., and Marin, G. B., *Catal. Lett.* **57**, 9 (1999).
- Dost, A. A., Dhanak, V. R., and Buckingham, S., *J. Catal.* **89**, 159 (1984).

- Ionnides, T., Efstatiou, A. M., Zhang, Z. L., and Verykios, X. E., *J. Catal.* **156**, 256 (1995).
- Anderson, J. A., and Khader, M. M., *J. Mol. Catal. A* **105**, 175 (1996).
- Gland, J., and Kollin, E. B., *J. Chem. Phys.* **78**, 963 (1983).
- Low, G. G., and Bell, A. T., *J. Catal.* **57**, 397 (1979).
- Sexton, B. A., and Somorjai, G. A., *J. Catal.* **46**, 167 (1977).
- Grünert, W., Wolf, D., Buyevskaya, O. V., Walter, K., and Baerns, M., *Z. Phys. Chem.* **197**, 49 (1996).
- Nieuwenhuys, B. E., *Surf. Sci.* **126**, 307 (1983).
- Finetti, P., Agostino, R. G., Derossi, A., Santoni, A., and Rosei, R., *Surf. Sci.* **262**, 1 (1992).
- Koel, B. E., Crowell, J. E., Bent, B. E., Mate, C. M., and Somorjai, G. A., *J. Phys. Chem.* **90**, 2949 (1986).
- Alstrup, I., Chorkendorff, I., and Ullmann, S., *Surf. Sci.* **293**, 133 (1993).
- Mikhailov, S. N., van den Oetelaar, L. C. A., Brongersma, H. H., and van Santen, R. A., *Catal. Lett.* **27**, 79 (1994).
- Borodzinski, A., *Polish J. Chem.* **72**, 2455 (1998).
- Padowitz, D. F., Peterlinz, K. A., and Sibener, S. J., *Langmuir* **7**, 2566 (1991).
- Padowitz, D. F., and Sibener, S. J., *J. Vacuum Sci. Technol. A* **9**, 2289 (1991).
- Colonell, J. I., Gibson, K. D., and Sibener, S. J., *J. Chem. Phys.* **103**, 6677 (1995).
- Padowitz, D. F., and Sibener, S. J., *Surf. Sci.* **254**, 125 (1991).
- Gibson, K. D., Colonell, J. I., and Sibener, S. J., *J. Chem. Phys.* **103**, 6735 (1995).
- Gibson, K. D., Viste, M., Sanchez, E. C., and Sibener, S. J., *J. Chem. Phys.* **110**, 2757 (1999).
- Colonell, J. I., Gibson, K. D., and Sibener, S. J., *J. Chem. Phys.* **103**, 6677 (1995).
- Schwartz, J. A., and Madix, R. J., *Surf. Sci.* **46**, 317 (1974).
- D'Evelyn, M. P., and Madix, R., *Surf. Sci. Rep.* **3**, 413 (1984).
- Jones, R. H., Olander, D. R., Siekhaus, W. J., and Schwarz, J. A., *J. Vacuum Sci. Technol. A* **9**, 1429 (1972).
- Harris, T. D., and Madix, R. J., *J. Catal.* **178**, 520 (1998).
- Peterlinz, K. A., Curtiss, T. J., and Sibener, S. J., *J. Chem. Phys.* **95**, 6972 (1991).
- Payne, S. H., Kreuzer, H. J., Peterlinz, K. A., Curtiss, T. J., Uebing, C., and Sibener, S. J., *Surf. Sci.* **272**, 102 (1992).
- Astaldi, C., Santoni, A., Della Valle, F., and Rosei, R., *Surf. Sci.* **220**, 322 (1989).
- Brown, L. S., and Sibener, S. J., *J. Chem. Phys.* **89**, 1163 (1988).